face. This fits with the transfer doping model, because it is conceivable that there would be no suitable molecules within the layer to contribute to the transfer doping process. The low content of hydrogen within the grain proves the potential of microwave CVD to grow high-quality diamond. The content is even well below the doping levels used for p and n doping of diamond and is, therefore, also in line with the high resistance of the studied sample.

References and Notes

1. B. Dischler, C. Wild, Eds., *Low-Pressure Synthetic Diamond,* vol. 11 of *Springer Series in Materials Processing,* W. Michaeli, H. Warlimont, E. Weber, Eds. (Springer, Berlin, 1998).
2. J. Isberg *et al.*, *Science* **297**, 1670 (2002).
3. A. Vescan, I. Daumiller, P. Gluche, W. Ebert, E. Kohn, *Diamond Relat. Mater.* **7**, 581 (1998).
4. E. Wörner, C. Wild, W. Müller-Sebert, P. Koidl, *Diamond Relat. Mater.* **10**, 557 (2001).
5. C. Manfredotti *et al.*, *Nucl. Instrum. Methods* **A458**, 360 (2001).
6. P. Bergonzo *et al.*, *Phys. Status Solidi* (*a*) **185**, 167 (2001).
7. J. C. Angus, C. C. Hayman, *Science* **241**, 913 (1988).
8. H. Kawarada *et al.*, *J. Appl. Phys.* **81**, 3490 (1997).
9. C. Yan, Y. K. Vohra, H. Mao, R. J. Hemley, *Proc. Natl. Acad. Sci. U.S.A.* **99**, 12523 (2002).
10. H. Kawarada, *Surf. Sci. Rep.* **26**, 205 (1996).
11. A. M. Stoneham, in *The Properties of Natural and Synthetic Diamond*, J. E. Field, Ed. (Academic Press, New York, 1992), pp. 4–34.
12. G. Dollinger, A. Bergmaier, C. M. Frey, M. Roesler, H. Verhoeven, *Diamond Relat. Mater.* **4**, 591 (1995).
13. F. Fuchs, C. Wild, K. Schwarz, W. Müller-Sebert, P. Koidl, *Appl. Phys. Lett.* **66**, 177 (1995).
14. C. Glover, M. E. Newton, P. Martineau, D. J. Twitchen, J. M. Baker, *Phys. Rev. Lett.* **90**, 185507 (2003).
15. B. Dischler, C. Wild, W. Müller-Sebert, P. Koidl, *Physica B* **185**, 217 (1993).
16. D. F. Talbot-Ponsonby *et al.*, *Phys. Rev. B* **57**, 2264 (1998).
17. R. D. Maclear *et al.*, *Diamond Relat. Mater.* **8**, 1615 (1999).
18. S. H. Connell *et al.*, *Diamond Relat. Mater.* **7**, 1714 (1998).
19. R. Samlenski, C. Haug, R. Delto, C. Wild, R. Brenn, *Nucl. Instrum. Methods* **B190**, 324 (2002).
20. D. Dujmić, M. Jakšić, N. Soić, T. Tadić, I. Bogdanović, *Nucl. Instrum. Methods* **B111**, 126 (1996).
21. K. A. Sjöland *et al.*, *Nucl. Instrum. Methods* **B124**, 639 (1997).
22. B. L. Cohen, C. L. Fink, J. H. Degnan, *J. Appl. Phys.* **43**, 19 (1972).
23. P. Reichart *et al.*, *Nucl. Instrum. Methods* **B219**, 980 (2004).
24. G. Datzmann *et al.*, *Nucl. Instrum. Methods* **B181**, 20 (2001).
25. Materials and methods are available on *Science* Online.
26. P. Reichart *et al.*, *Nucl. Instrum. Methods* **B197**, 134 (2002).
27. C. Wild, N. Herres, P. Koidl, *J. Appl. Phys.* **68**, 973 (1990).
28. F. Maier *et al.*, *Surf. Sci.* **443**, 177 (1999).
29. A. Bergmaier, G. Dollinger, A. Aleksov, P. Gluche, E. Kohn, *Surf. Sci.* **481**, L433 (2001).
30. G. J. Feldman, R. D. Cousins, *Phys. Rev. D* **57**, 3873 (1998).
31. S. M. Hearne, D. N. Jamieson, E. Trajkov, S. Prawer, J. E. Butler, *Appl. Phys. Lett.* **84**, 4493 (2004).
32. C. E. Nebel *et al.*, *Appl. Phys. Lett.* **79**, 4541 (2001).
33. F. Maier, M. Riedel, B. Mantel, J. Ristein, L. Ley, *Phys. Rev. Lett.* **85**, 3472 (2000).

34. This work was supported by the Beschleunigerlaboratorium der LMU und TU München, as well as the German Bundesministerium für Bildung und Forschung. We thank T. Graf, WSI München, and L. Goergens; TU München, for the atomic force microscopy and x-ray diffraction measurements, as well as M. Schubert, LMU München, and A. Bergmaier; TU München, for data acquisition and programming support. Many thanks also to R. Lutter, O. Schaile, K. Steinberger, LMU München, and the whole accelerator team for their great assistance.

Supporting Online Material

www.sciencemag.org/cgi/content/full/306/5701/1537/DC1
Materials and Methods
Figs. S1 to S5
References and Notes

19 July 2004; accepted 7 October 2004

Probing Electronic Transitions in Individual Carbon Nanotubes by Rayleigh Scattering

Matthew Y. Sfeir,[1]* Feng Wang,[2]* Limin Huang,[3] Chia-Chin Chuang,[4] J. Hone,[4] Stephen P. O'Brien,[3] Tony F. Heinz,[2]† Louis E. Brus[1]†

Rayleigh scattering spectra were obtained from individual single-walled carbon nanotubes with the use of a laser-generated visible and near-infrared supercontinuum. This diagnostic method is noninvasive and general for nanoscale objects. The approach permits clear identification of excited states in arbitrary metallic and semiconducting nanotubes. We analyzed spectral lineshapes in relation to the role of excitonic effects and correlated the results with Raman scattering data on individual tubes. The nanotube structure remained the same over distances of tens of micrometers. Small nanotube bundles retained distinct Rayleigh spectroscopic signatures of their component nanotubes, thus allowing the probing of nanotube-nanotube interactions.

Single-walled carbon nanotubes (SWNTs) comprise a family of more than 200 structures characterized by different chiral angles and diameters, each having a distinct electronic structure that can be either metallic or semiconducting (*1*). This richness and diversity, which makes carbon nanotubes so promising for various applications (*2–4*), poses a substantial challenge in characterization of specific SWNTs. A general optical characterization technique that permits noninvasive measurements of the electronic structure of an arbitrary individual nanotube has been lacking. Among existing techniques, vibrational spectra of individual SWNTs have been obtained from resonance Raman scattering (*5–7*). Although Raman excitation spectra provide some information on the electronic transitions, the requirement of tunable excitation and the weakness of the Raman signal make these experiments extremely challenging (*8*). Recent observations of nanotube fluorescence, and the corresponding excitation spectra, have furthered the characterization of SWNTs (*9–11*). However, this approach is inherently limited to semiconducting nanotubes and its application is currently restricted to small-diameter tubes.

We use Rayleigh scattering spectroscopy to identify the electronic transitions of both metallic and semiconducting individual nanotubes. Rayleigh scattering—the ubiquitous process of elastic light scattering from a small, polarizable object—provides spectroscopic information about the system through the scattering resonant enhancement when the photon energy matches that of an electronic transition. Rayleigh scattering occurs whether or not the sample luminesces, and it is intrinsically stronger than inelastic Raman scattering because it does not require the incident light to couple to the vibrations of the system. As such, the approach should be broadly applicable for probing an arbitrary nanoscale object. When implemented with a bright white-light source, the technique offers sufficient versatility and speed to probe spatially localized regions along an individual nanotube, as well as tube-tube interactions in bundles. The method can be easily combined with other types of single-nanotube measurements.

Rayleigh scattering is normally not considered for nanoscale objects because of the expectation that signals will be extremely weak. However, we report that Rayleigh scattering spectra from individual SWNTs can be obtained with high signal-to-noise ratio in less than 1 min with a white-light source of laser brightness. The white-light

[1]Department of Chemistry, [2]Departments of Physics and Electrical Engineering, [3]Department of Applied Physics and Applied Mathematics, [4]Department of Mechanical Engineering, Columbia University, 3000 Broadway, New York, NY 10027, USA.

*These authors contributed equally to this work.
†To whom correspondence should be addressed. E-mail: tony.heinz@columbia.edu, leb26@columbia.edu

supercontinuum is generated by passing femtosecond laser pulses from the output of a mode-locked Ti:sapphire laser operating at a wavelength of 800 nm through a microstructured optical fiber. The nonlinear response of the fiber yields radiation covering a spectral range of ~450 to 1550 nm with an average power of tens of mW (*12*).

To minimize background scattering and to produce nanotubes free from the local perturbations of a substrate, we used standard optical lithography and wet etching procedures to prepare slits (width 30 μm, length 1 mm) etched completely through a silicon substrate. SWNTs were prepared using a chemical vapor deposition process in which the flow of the carbon feed gas was arranged to yield directionally controlled growth of SWNTs across the slit (Fig. 1) (*13*). Various catalysts and feed gases were used (*14*–*16*), with the catalyst density chosen so that about 20 nanotubes, typically well separated from one another, were grown along the length of the slit.

The white light is focused with a microscope objective to ~2 μm^2 at the slit and is directed at normal incidence onto a suspended SWNT. The scattered light is collected at an oblique angle in a confocal arrangement and is analyzed with a spectrograph equipped with a two-dimensional charge-coupled device (CCD) array. The Rayleigh scattering spectra are then obtained after correction for the profile of the supercontinuum light and the detection sensitivity of the system. The incident supercontinuum light is filtered to remove the infrared component and attenuated to an average power of a few mW, comparable to what is typically used in Raman scattering experiments. Under these conditions, possible contributions from nonlinear and thermal effects are ruled out experimentally because the Rayleigh scattering spectra are independent of excitation intensity. Rayleigh scattering data in the spectral range of 450 to 850 nm were recorded with integration times of 10 to 30 s. Complementary resonance Raman spectra in a backscattering geometry (*6*) were obtained for selected SWNTs; we used a few mW of 1.96-eV laser radiation and holographic notch filters to reject the elastic Rayleigh component. Data collection times for the resonance Raman scattering typically exceeded those for Rayleigh scattering by a factor of 100.

By comparing the results of scanning electron microscopy (SEM, Fig. 1A) to those for Rayleigh scattering (Fig. 1B), we found that we detected scattering from all of the suspended tubes—both metallic and semiconducting isolated tubes as well as small bundles. This result contrasts with the case of fluorescence, for which only isolated single semiconducting tubes are observable. In the optical image, the bright center spot is the elastic scattering of the focused supercontinuum from an individual suspended SWNT, shown in a color that represents the specific wavelength of the nanotube resonant response. The white lines above and below this region arise from scattering of stray supercontinuum light from the slit edges.

Representative experimental Rayleigh scattering spectra (Fig. 2) comprise well-defined and highly reproducible peaks that reflect the optical transitions of the SWNT under study. The resolution of our experiment is sufficient to distinguish between two peaks separated by as little as 5 meV. The ~50 individual SWNTs observed display the basic motifs of Fig. 2A, with two well-resolved and separated peaks, or of Fig. 2B, with one broad or slightly split peak. The electronic states of the periodic SWNT structure have band-like character, with successive bands indexed by the angular quantization number around the nanotube. Because of their quasi–one-dimensional nature, the density of states exhibits a van Hove singularity at the onset of each energy band, as shown schematically in Fig. 2, A and B. Within a free-carrier picture of the optical excitation, the sharp resonances in the Rayleigh scattering spectrum arise from the singularity in the joint density of states (JDOS) for transitions between two bands. The energy of these transitions varies with the nanotube diameter and helicity in a

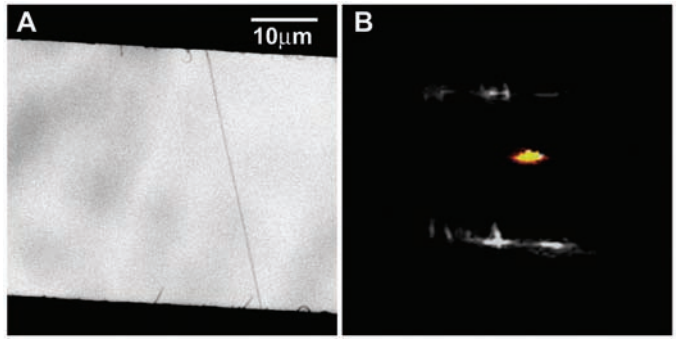

Fig. 1. Images of a suspended isolated carbon nanotube. (**A**) SEM image showing the silicon substrate (upper and lower dark areas) and the isolated carbon nanotube that spans the slit. Small sections of other nanotubes are also visible at the slit edges. (**B**) Rayleigh scattering imaged on a CCD camera. The suspended nanotube is excited by supercontinuum light in the center of the slit, leading to observable scattered radiation, as shown here in a color corresponding to the electronic resonance. The edges of the slits, represented in white, are visible because of scattering of background light.

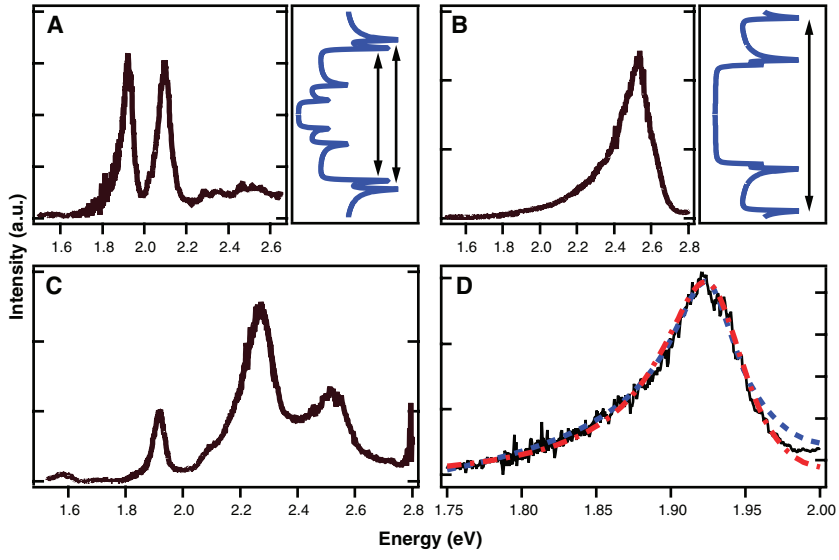

Fig. 2. Rayleigh scattering spectra. (**A**) Spectrum of an isolated SWNT showing the E_{33} and E_{44} transitions of a semiconducting nanotube. The instrumental resolution is 5 meV. The density of states (with van Hove singularities) of a similar semiconductor nanotube is illustrated at the right; arrows represent assigned transitions. (**B**) Spectrum from the E_{22} transition of a metallic carbon nanotube. The broader linewidth is attributed to lifetime broadening or unresolved splitting caused by the trigonal warping effect. The density of states is shown at the right; an arrow illustrates the assigned transition for a similar nanotube. (**C**) Spectrum of a small carbon nanotube bundle. This type of spectrum is easily distinguishable from that of a single isolated tube. (**D**) Fit of lower energy peak in (A) to the free-carrier (blue dashed line) and excitonic (red dot-dashed line) models discussed in the text.

characteristic fashion (*1*, *17*). We assign the two separated peaks to the E_{33} and E_{44} transitions of an individual semiconducting tube, and the single broadened peak to the E_{22} transition of an individual metallic tube, as expected for SWNTs in the 1.7-nm diameter range that is typically obtained in our synthesis. The much larger apparent width of the metallic transition could be due to lifetime broadening from the shorter-lived excited state. It may also be the result of two closely positioned peaks, which are sometimes resolvable experimentally, associated with the trigonal warping effect (*6*, *18*). In addition to the individual SWNT spectra, we observe Rayleigh scattering with increased strength and spectral complexity that we assign to bundles of SWNTs. A representative example in which the spectrum reflects the presence of two SWNTs (Fig. 2C) illustrates a unique feature of our technique: It can readily distinguish between small bundles and individual nanotubes, while still retaining the capability to reveal distinct spectral features of each species.

We probe the local response in different spatial regions by moving the focus of the white-light supercontinuum along a given SWNT. As an example, Fig. 3A shows Rayleigh scattering spectra taken at the two ends of a particular suspended nanotube. It is expected that because SWNTs are in a robust and stable configuration, they retain their specific chirality for the entire length. There is, however, little direct experimental evidence to support this widely held hypothesis. The excellent match of the Rayleigh scattering spectra of Fig. 3A shows unambiguously that the SWNT retains precisely the same chirality and diameter over the 30-μm separation, a distance corresponding to more than 1 million carbon atoms in the nanotube.

Resonant Rayleigh scattering provides information about both the energies and lineshapes of the electronic transitions. We model the Rayleigh scattering from an individual SWNT as electromagnetic scattering from an infinite right cylinder. The scattering cross section per unit length is $\sigma(\omega) \propto r^4\omega^3|\varepsilon(\omega) - 1|^2$ (*19*), where ω is the frequency of the scattered light, r is the radius of the cylinder, and $\varepsilon(\omega)$ is the effective dielectric function of the nanotube. The features of the Rayleigh spectra arise from the frequency-dependent dielectric function, which in turn reflects the wave functions and electronic transitions.

One of the major outstanding issues concerning optically excited states in SWNTs is the importance of the electron-hole interaction. For weak interactions, an optical transition generates free electrons and holes, as would generally be the case for bulk three-dimensional semiconductors at room temperature. In quasi–one-dimensional systems such as SWNTs, however, electron-hole interactions are expected to be enhanced, and theoretical studies suggest the formation of excitons rather than free carriers (*20*–*22*). In this context, we compare the experimental lineshapes with the predictions for free-carrier and excitonic transitions. In Fig. 2D we show a detail of the Rayleigh scattering spectrum for the lower energy feature in Fig. 2A, which has a linewidth (full width at half-maximum) of ~55 meV. The shape of other measured transitions is quite similar. To analyze the data, we consider the free-carrier response to be dominated by the van Hove singularity in the JDOS (*17*) and consider the excitonic response to feature a Lorentzian resonance of a width chosen to fit the experimental data. An arbitrary, spectrally flat component is included in the real part of the dielectric function for both models to account for the nonresonant contribution to the scattering from other electronic transitions in the SWNT. Interestingly, we find (Fig. 2D) that both models are compatible with the experimental data. The required phenomenological broadening in the two pictures (20 meV and 35 meV, respectively) is, however, significantly different. Theoretical studies that provide a reliable prediction for the broadening should consequently be able to discriminate between these two pictures, using the experimental lineshapes reported here.

The well-defined experimental geometry also allows us to examine the polarization properties of the Rayleigh scattering process. Shown in Fig. 3B is the Rayleigh scattering amplitude as a function of the scattered light polarization; the same effect is measured when varying the polarization of the incident supercontinuum radiation. The strongest scattering is achieved when the incident light and scattered light are polarized parallel to the tube. The polarization dependence follows closely the $\cos^2\theta$ form expected for dipole emission along the nanotube axis. As indicated in Fig. 3A, however, weak Rayleigh scattering can be seen for incident light polarized perpendicular to the nanotube axis. The spectra of light scattering when polarized along the nanotube obey the selection rule of $\Delta J = 0$ (i.e., symmetric transitions between the valence and conduction energy bands with the same band index J), such as the above-mentioned E_{22}, E_{33}, and E_{44} transitions. When the electric field is perpendicular to the nanotube axis, the tight-binding model predicts selection rules allowing for $\Delta J = 1$ transitions of comparable strength (*23*). We observe behavior that reflects the role of the depolarization or "antenna" effect (*24*), essentially a manifestation of the ability of a SWNT to act like a macroscopic object in perturbing the incident light through strong local-field screening of the perpendicular component of the exciting electric field. Although previous experimental results of Rayleigh scattering on large bundles and Raman scattering (*25*, *26*) provided evidence of this effect, other investigations have suggested that $\Delta J = 1$ transitions play a role in resonance Raman scattering in nanotubes (*27*). Our measurements on aligned individual nanotubes pro-

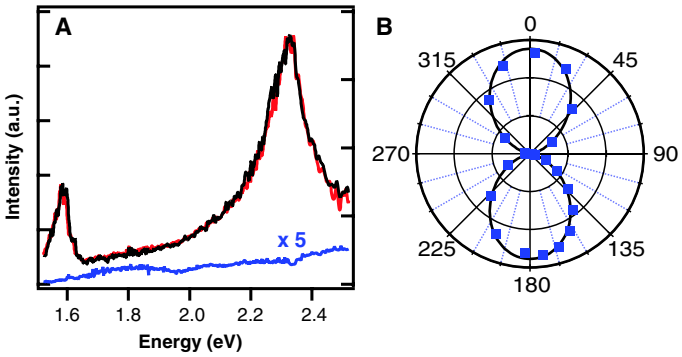

Fig. 3. Polarization dependence of the Rayleigh scattering. (**A**) The black line is the spectrum obtained from one end of the nanotube when the incident light is polarized parallel to the tube axis. The red line shows the identical spectrum obtained from the opposite end of the suspended tube ~30 μm away. The blue spectrum (magnification ×5) is obtained for incident light polarized perpendicular to the axis of the nanotube. (**B**) Rayleigh scattering intensity as a function of the angle between the electric field polarization and the tube axis. The solid line is a $\cos^2\theta$ fit.

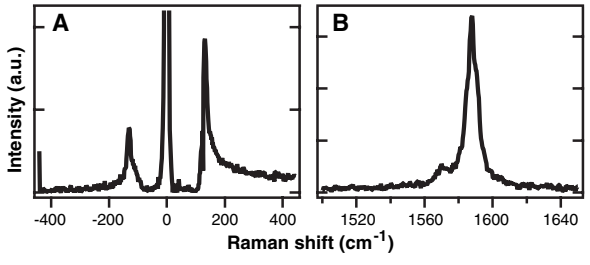

Fig. 4. Resonance Raman scattering spectra for the SWNT of Fig. 2A obtained with excitation at a photon energy of 1.96 eV. (**A**) Stokes and anti-Stokes Raman spectra of the RBM. The instrumental resolution is less than 3 cm^{-1}. The frequency of this mode implies a diameter of 1.89 nm. (**B**) Raman spectrum of the G-mode.

vide a direct demonstration of the dominant role of local-field screening.

The Rayleigh spectra provide information that can guide other optical measurements. The Rayleigh data are particularly useful for Raman scattering, which requires an electronic resonance to make measurements from an individual SWNT. Shown in Fig. 4 are resonance Raman spectra for the same SWNT examined in Fig. 2A by Rayleigh scattering. The Rayleigh spectrum was recorded first and found to have resonances at 1.92 and 2.10 eV; we were then able to choose the Raman laser excitation energy (1.96 eV) to match one of the observed transitions. Without such prior knowledge of the resonance energy, experiments must rely on a difficult and time-consuming trial-and-error approach using available laser excitation wavelengths (*28*). Raman measurements provide additional structural information about SWNTs through the sensitivity of the vibrational modes on the nanotube diameter and chirality (*6*, *18*). We collected both Stokes and anti-Stokes Raman spectra of the radial breathing mode (RBM) (Fig. 4A) as well as the Stokes Raman spectrum of the carbon-carbon stretch G-mode (Fig. 4B). According to the formula relating the Raman shift of the RBM mode frequency (ω_{RBM}) to nanotube diameter (d_t) (*7*), $\omega_{RBM} = 248/d_t$, the diameter of this nanotube is 1.89 nm. We then assigned the transitions on the basis of the qualitative pattern of close-lying E_{44} (2.10 eV) and E_{33} (1.92 eV) transitions with a large gap to an unobserved E_{22} transition lying below 1.4 eV, as predicted by tight-binding theory for semiconducting tubes near 1.89 nm (*1*, *29*). This may be the nanotube with a diameter of 1.85 nm and chiral indices of (21, 4). We calculate that this tube would have Rayleigh peaks at 0.88, 1.87, and 2.10 eV for a γ_o value (the overlap integral between nearest neighboring atomic sites) of 2.89 eV.

The effectiveness of the characterization of nanoscale objects by Rayleigh scattering with high-brightness white light is apparent from this initial report. We expect that the approach will permit optical probing of a wide variety of other individual nanoscale structures. In the context of carbon nanotubes, a systematic study should yield firm assignments for the entire family of semiconducting and metallic nanotubes. This will permit complementary investigations of transport, mechanical, and chemical properties of nanotubes to be conducted with a convenient spectroscopic identification of the precise structure of the nanotube under study, thus alleviating one of the major limitations of current studies.

References and Notes

1. R. Saito, G. Dresselhaus, M. S. Dresselhaus, *Physical Properties of Carbon Nanotubes* (Imperial College Press, London, 1998).
2. M. M. J. Treacy, T. W. Ebbesen, J. M. Gibson, *Nature* **381**, 678 (1996).
3. S. J. Tans, A. R. M. Verschueren, C. Dekker, *Nature* **393**, 49 (1998).
4. P. Kim, L. Shi, A. Majumdar, P. L. McEuen, *Phys. Rev. Lett.* **87**, 215502 (2001).
5. G. S. Duesberg, I. Loa, M. Burghard, K. Syassen, S. Roth, *Phys. Rev. Lett.* **85**, 5436 (2000).
6. Z. Yu, L. E. Brus, *J. Phys. Chem. B* **105**, 6831 (2001).
7. A. Jorio *et al.*, *Phys. Rev. Lett.* **86**, 1118 (2001).
8. A. Jorio *et al.*, *Phys. Rev. B* **63**, 245416 (2001).
9. M. J. O'Connell *et al.*, *Science* **297**, 593 (2002).
10. A. Hartschuh, H. N. Pedrosa, L. Novotny, T. D. Krauss, *Science* **301**, 1354 (2003).
11. J. Lefebvre, Y. Homma, P. Finnie, *Phys. Rev. Lett.* **90**, 217401 (2003).
12. J. C. Knight, T. A. Birks, P. S. J. Russell, D. M. Atkin, *Opt. Lett.* **21**, 1547 (1996).
13. S. Huang, X. Cai, J. Liu, *J. Am. Chem. Soc.* **125**, 5636 (2003).
14. C. L. Cheung, A. Kurtz, H. Park, C. M. Lieber, *J. Phys. Chem. B* **106**, 2429 (2002).
15. L. An, J. M. Owens, L. E. McNeil, J. Liu, *J. Am. Chem. Soc.* **124**, 13688 (2002).
16. S. Maruyama, R. Kojima, Y. Miyauchi, S. Chiashi, M. Kohno, *Chem. Phys. Lett.* **360**, 229 (2002).
17. M. F. Lin, K. W. K. Shung, *Phys. Rev. B* **50**, 17744 (1994).
18. R. Saito *et al.*, *Phys. Rev. B* **64**, 085312 (2001).
19. C. F. Bohren, D. R. Huffman, *Absorption and Scattering of Light by Small Particles* (Wiley, New York, 1983).
20. T. Ando, *J. Phys. Soc. Jpn.* **66**, 1066 (1997).
21. C. L. Kane, E. J. Mele, *Phys. Rev. Lett.* **90**, 207401 (2003).
22. C. D. Spataru, S. Ismail-Beigi, L. X. Benedict, S. G. Louie, *Phys. Rev. Lett.* **92**, 077402 (2004).
23. M. F. Lin, *Phys. Rev. B* **62**, 13153 (2000).
24. H. Ajiki, T. Ando, *Physica B* **201**, 349 (1994).
25. Z. H. Yu, L. Brus, *J. Phys. Chem. B* **105**, 1123 (2001).
26. A. Jorio *et al.*, *Phys. Rev. B* **65**, 121402 (2002).
27. A. Jorio *et al.*, *Phys. Rev. Lett.* **90**, 107403 (2003).
28. C. Fantini *et al.*, *Phys. Rev. Lett.* **93**, 087401 (2004).
29. R. Saito, G. Dresselhaus, M. S. Dresselhaus, *Phys. Rev. B* **61**, 2981 (2000).

30. We thank M. Hybertsen, X. Cui, G. Dukovic, I. Mandelbaum, and V. Perebeinos for helpful discussions and O. Cherniavskaya for assistance with sample growth and characterization. Supported by the NSF Nanoscale Science and Engineering Initiative (grant CHE-0117752), the New York State Office of Science, Technology, and Academic Research (NYSTAR), and the Office of Basic Energy Sciences, U.S. Department of Energy (grants DE-FG02-98ER 14861 and DE-FG02-03ER 15463).

27 July 2004; accepted 5 October 2004
Published online 28 October 2004;
10.1126/science.1103294
Include this information when citing this paper.

Seismic Anisotropy Beneath Ruapehu Volcano: A Possible Eruption Forecasting Tool

Alexander Gerst[1,2]*† and Martha K. Savage[1]

The orientation of crustal seismic anisotropy changed at least twice by up to 80° because of volcanic eruptions at Ruapehu Volcano, New Zealand. These changes provide the basis for a new monitoring technique and possibly for future midterm eruption forecasting at volcanoes. The fast anisotropic direction was measured during three seismometer deployments in 1994, 1998, and 2002, providing an in situ measurement of the stress in the crust under the volcano. The stress direction changed because of an eruption in 1995–1996. Our 2002 measurements revealed a partial return to the pre-eruption stress state. These changes were probably caused by repeated filling and depressurizing of a magmatic dike system.

About 10% of the world's population live near an active volcano and are therefore threatened by volcanic eruptions (*1*). More tools are needed to fill in the gap between short-term eruption forecasting (days to weeks) and long-term forecasting (several years) to provide information about the future onset of an eruption and the current state of the volcano within an eruption cycle (*2*). The method of shear-wave splitting analysis at volcanoes has the potential to provide a new tool for midterm eruption forecasts (months to years).

Mount Ruapehu is the largest andesite-dacite volcano in New Zealand. Eruptions have caused the loss of life and property and are likely to recur in the near future. In 1995 and 1996, the largest historical eruption of Ruapehu took place with little warning, ejecting a volume of material of about 0.05 km^3, producing a 12-km-high volcanic plume, sending major lahars down the flanks (*3*, *4*), and producing economic damage of about US$50 million (*5*). Major eruptions also occurred in 1945, 1969, 1975, 1981, and 1988, many with little or no warning.

Volcanic eruptions are almost always preceded by magma movements in the feeder

[1]Institute of Geophysics, School of Earth Sciences, Victoria University of Wellington, New Zealand. [2]University of Karlsruhe, Germany.

*Present address: Institute of Geophysics, University of Hamburg, Bundesstrasse 55, 20146 Hamburg, Germany.
†To whom correspondence should be addressed. E-mail: publications@planet3.de